Studies on Crystallization Behaviors and Crystal Morphology of Polyamide 66/Clay Nanocomposites

Xin Kang, Suqin He, Chengshen Zhu, Liuyang Wangm Liyun Lǔ, Jianguo Guo

Faculty of Materials Engineering, Zhengzhou University, Zhengzhou 450052, China

Received 6 October 2003; accepted 1 August 2004
DOI 10.1002/app.21257
Published online in Wiley InterScience (www.interscience.wiley.com).

ABSTRACT: X-ray diffraction methods, DSC thermal analysis, and polarized light microscopy (PLM) were used to investigate the structural changes of nylon 66/clay nanocomposites. PA 66/clay nanocomposites were prepared by the method of melt intercalation. The results indicate that the addition of the intercalated organo-montmorillonite (OMMT) can induce generation of the β-form crystal of PA 66 and substantially affect the arrangement of molecules in the α-form crystal, although the crystallinity scarcely changes. Also, the DSC results indicate that the addition of OMMT in the PA 66 matrix leads to increases of crystallization temperatures and the full width at half maximum (FWHM) of the exothermic peaks. Moreover, the viscosity factor is the main influence on FWHM of the exothermic peaks of PA 66/clay nanocomposites. The results of nonisothermal crystallization kinetics show that OMMT has the effect of heterogeneous nucleation and leads to the decrease of the size of the spherocrystal. The heterogeneous nucleation effects of OMMTs influence the mechanism of crystallization and the growth mode of PA 66 crystals. PLM photographs verify that the size of spherocrystal is decreased and visually confirm the theory of crystallization kinetics.
 J Appl Polym Sci 95: 756–763, 2005

Key words: crystallization; kinetics (polym.); montmorillonite; polyamide 66; nanocomposites

INTRODUCTION

The recent interest in polymer/clay nanocomposites (PCN) stems from the dramatic improvement on their thermal and mechanical properties that can be produced by adding just a small fraction of clay to a polymer matrix.[1] The majority of recent work on PCN has focused on synthesis and characterization of physical properties. Although the improved properties were achieved, the fundamental mechanisms for property enhancements in the nanocomposites are not well understood. It is complicated to establish the structure–property relationship because there may exist a number of morphological and processing factors that influence both the inorganic filler and polymer, such as the orientation of the silicate layers and the influence of silicate layers on polymer conformation and morphology.[2,3] For the PCN with a semicrystalline polymer matrix, this problem becomes even more complicated because the addition of silicate layers has an impact not only on the conformation and morphology of polymer chains, but also on the crystalline structure. As a typical example, polyamide 6/clay nanocomposites, perhaps the most successful system so far demonstrating dramatic improvement in properties, has been extensively reported with respect to the crystallization behaviors and crystal morphology. However, there are few studies about the crystallization behaviors of PA 66/clay nanocomposites. In this article, we report our results on the crystallization behaviors and crystal morphology.

Correspondence to: C. Zhu (zhucs@zzu.edu.cn).

Journal of Applied Polymer Science, Vol. 95, 756–763 (2005)

EXPERIMENTAL

Materials

The montmorillonite (MMT) used in this experiment was supplied by the Institute of Chemical Metallurgy, Chinese Academy of Sciences. MMT is a natural clay mineral with a cation exchange capacity of 100 meq/100 g. PA 66, with a relative viscosity of 3.22, was purchased from China Shenma Group Nylon 66 Salt Co. Ltd. Cetyltrimethylammonium bromide (CTAB) was purchased from Tianning Chemical Reagent Co. (Jining City, Qinghai Province, China).

Preparation of composites

A 15-g sample of CTAB was dispersed in 300 mL warm distilled water, and the solution was blended with a 1000-mL suspension of layered clay, with stirring, at 65°C. The mixture was stirred at 65°C for 3 h. Then it was washed and filtrated under vacuum and the sediments were dried under vacuum at 100°C for 10 h. The sediments were modified with nylon 6, and the products were dried under vacuum at 100°C for 12 h.

Pellets of PA 66 and organo-montmorillonite (OMMT) were melt-blended at 260–280°C using a TE-34 twin-screw extruder (Institute of Extrusion Machine, Institute of Chemical Machines, Department of Chemical Industry of China) to yield the composites. The obtained strands were pelletized and dried under vacuum at 90°C. The samples, of which the clay contents were 1, 3, 5, 7, and 9 phr, were designated as PCN-01, PCN-02, PCN-03, PCN-04, and PCN-05, respectively. The dried pellets of the composites were hot pressed into thin films at 290°C and maintained for 10 min at 240°C. Then, samples were cooled slowly from the melt to room temperature in ambient air. Pure PA 66 was designated as PCN-06.

Characterization

Wide-angle X-ray diffraction (WAXD) patterns were recorded by monitoring the diffraction angle 2θ from 10 to 40° on a D/MAX-IIIB X-ray diffractometer (Rigaku, Tokyo, Japan) using Cu–K_α radiation (λ = 0.154 nm) operated at 35 kV and 30 mA, at a scanning rate of 4°/min. The specimen was made into a 1 × 1 × 0.05-cm lamella.

DSC thermal analysis was performed using a Netzsch TG209 instrument (Netzsch-Gerätebau GmbH, Bavaria, Germany) at a heating rate of 10°C/min to 285°C and holding for 5 min, and then cooling the samples to 20°C at a rate of 10°C/min under N_2 atmosphere. The curves of fusing and crystallization were recorded.

Photographs of these samples, obtained by polarized light microscopy (PLM), were obtained using a Xintian XP3C polarized light microscope. The mechanical properties of samples are detailed in our previous work.[4]

The melt indices of PA 66 and its nanocomposites were determined on a μPXRZ-400C melt flowing rate determinator using a 1-kg load at 270°C.

RESULTS AND DISCUSSION

Qualitative identification of crystalline forms of PA 66 and its nanocomposites

Polyamides exist in different polymorphic crystalline structures. The most important phases are the monoclinic α-form and pseudohexagonal γ-form for polyamide 6 (PA 6) and triclinic α-form and β-form for polyamide 66 (PA 66).[5–8]

The lower-temperature α-phase in PA 66 is composed of chain-folded sheets and is a consequence of the linear hydrogen bonds, induced by the progressive shear of chains, between amide groups in the adjacent chains within the sheet. The higher-temperature β-phase in the PA 66 consists of pleated sheets of chains joined by hydrogen bonds in which the intersheet shear of chains occurs alternately in the *c*-direction rather than progressively.

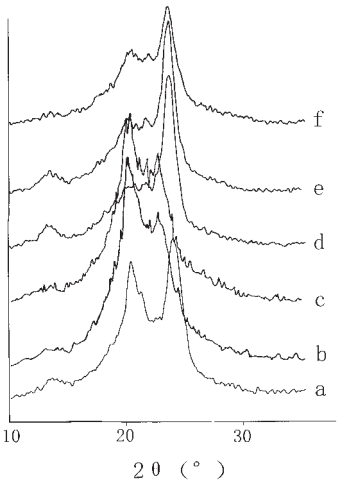

Figure 1 WAXD pattens of PA 66 and its nanocomposites: (a) PCN-06; (b) PCN-01; (c) PCN-02; (d) PCN-03; (e) PCN-04; (f) PCN-05.

Murthy et al.,[9] using nuclear magnetic resonance spectroscopy (NMR) and X-ray diffraction (XRD) measurements during heating PA 66 and PA 6, first reported the presence of a crystal–crystal transition called the Brill transition. The Brill transition in PA 66 has been studied extensively for many polyamides.[10–13] The room-temperature triclinic α-form structure transforms into a high-temperature triclinic β-form structure at elevated temperatures in PA 66. The Brill transition in PA 66 can be displayed clearly in XRD studies: two intense reflections at 21 and 24° merge into a single reflection at 21.5° during the transition.[14]

WAXD patterns of PA 66 and its nanocomposites crystallized from the melt at 240°C are shown in Figure 1. The PA 66 (PCN-06) may contain multicrystalline forms but only two α-crystalline peaks at 20.5 and 24° are visible. Following the addition of OMMT into the PA 66 matrix, the XRD shows a weak crystalline peak at 21.5° and that peak is increased with increasing OMMT contents. That crystalline peak can be caused by the appearance of the β-form crystal of PA 66 or by the γ-form crystal of PA 6. PA 6 was used as surface-active agent of MMT here and the usage level of PA 6 is 50% of the weight of MMT, that is to say, PA 6 is less than 4.5% of the weight of PA 66. However, according to Wu and Wu,[15] the γ-form crystalline peak of PA 6/clay nanocomposites will disappear when the clay content is 2.5 wt %. Therefore, the weak peak at 21.5° belongs to the β-form crystal of PA 66, which is induced by the addition of OMMT.

The nucleating effect of OMMT on the β-form crystal of PA 66 is probably attributable to the structural features of the silicate layers of MMT and its hetero-

geneous nucleation effect. As seen from the TEM photograph of PA 66/clay nanocomposites,[4] the multilayer structure of OMMT in the matrix is orderly in the short range but random in the long range.

According to Nylon Plastics[16] and the work of Keller and Maradudin,[17] the β-form of PA 66 amounts to a slight perturbation of the α-phase and the interpretation postulates initial stages of ordering and the presence of unrelated small crystallites. Thus, the presence of the β-form cannot be reliably determined except in samples possessing a high degree of axial orientation and the two phases probably represent stages in a continuum of possible states of order.

In the nanocomposite systems, the multilayer structure of MMT can cause the molecular chains of PA 66 to orient on the *c*-direction at a high degree. Moreover, the MMT crystals also presented in the matrix before PA 66 crystallized, which was small and unrelated to the PA 66 crystal. Therefore, the existence of MMT results in the generation of the β-form crystal of PA 66.

In addition, the XRD data exhibit a change of the intensities of the two α-crystalline peaks with increasing clay contents. The results indicate that a sharp α-crystalline peak at 20.5° and the trace of another α-crystalline peak at 24° are found when the clay contents are less than 3 phr, whereas the situation is opposite when the clay contents are greater than 3 phr. The phenomenon is related to the alignment modes of chains of PA 66 on the surfaces of silicate layers by surface-active agents with specific structures. The chains of PA 66 are compatible with the organic parts of those surface-active agents and the hydroxyl groups of the molecular chains of PA 66 undergo a chemical reaction with the organic parts, according to the principle of the selection of surface-active agents.[18–21] That is to say, the surfaces of silicate layers are possibly a vertical plane of the *a*–*c* plane of the PA 66 crystal, in which hydrogen bonds are in parallel arrangement.

Figure 2(a) gives a model of the arrangement of chains of PA 66 on the surface of a silicate layer. According to work of Brill,[10] the peak at 20.5° of WAXD corresponds to the (200) planes of PA 66 crystals, whereas the peak at 24° corresponds to the (002) and (202) planes. Figure 2(b) shows the principal crystallographic planes of PA 66. As seen in Figure 2(a), when the clay content is low, the permeation of bulk polymers leads to disorder and separation of silicate layers, that is, the pellets of MMT are exfoliated. Then, most of PA 66 molecular chains can align only on the *a*-direction of the PA 66 crystal, that is, the alignment direction of (200) planes during the crystal formation. That leads to the increase of the intensity of α-crystalline peak at 20.5°. However, when there are enough silicate layers, the permeation of polymers can only result in finite expansion of silicate layers and generate intercalated nanocomposites, in which chains of

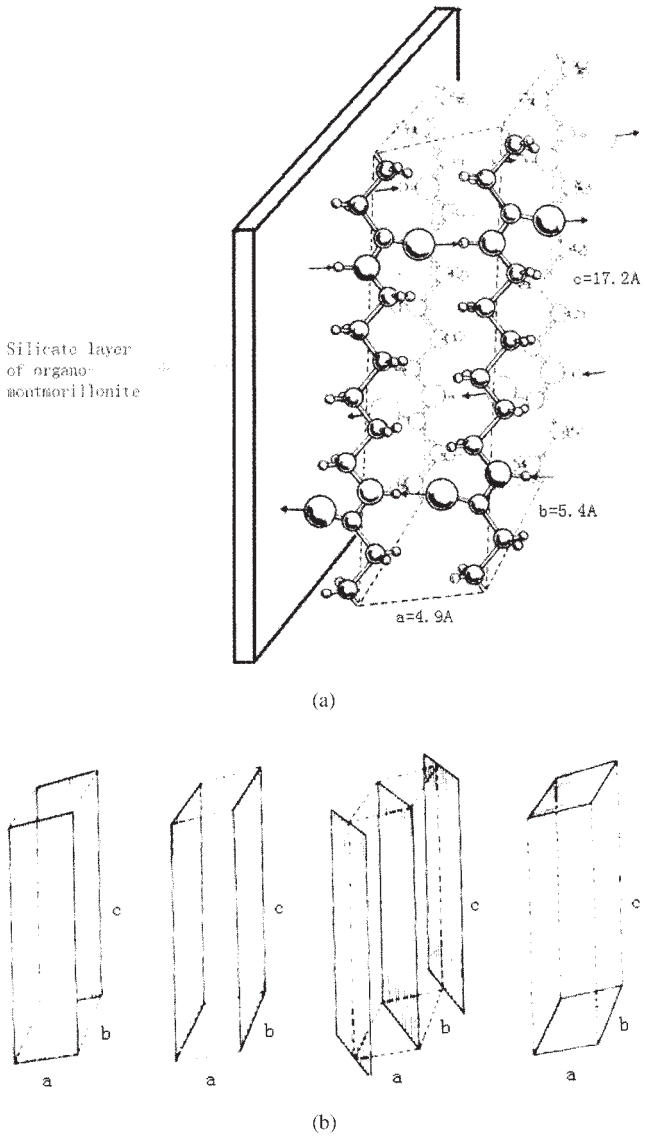

Figure 2 (a) Model of the arrangement of chains of PA 66 on the surface of a silicate layer. (b) Principal crystallographic planes of PA 66.

polymers will align on the axial direction of polymers. For PA 66, the axial direction of molecular chains is the alignment direction of (002) planes. Therefore, intensity of the diffraction peak at 24° is increased with increasing clay content. With a further increase of clay contents, the large quantity of clay will agglomerate and the orientation of PA 66 chains between the silicate layers will be decreased, so the intensity of the peak at 24° will be weakened.

From the above discussion, it is clear that the addition of MMT can induce the generation of β-form crystals of PA 66 and substantially affect the arrangement of molecules in α-form crystals. However, crystallinities of PCN-06 and PCN-03, calculated by the data of Figure 1, are 24.3 and 24.8%, respectively. That is to say, the addition of clay does not affect the crystallines of PA 66 and its nanocomposites.

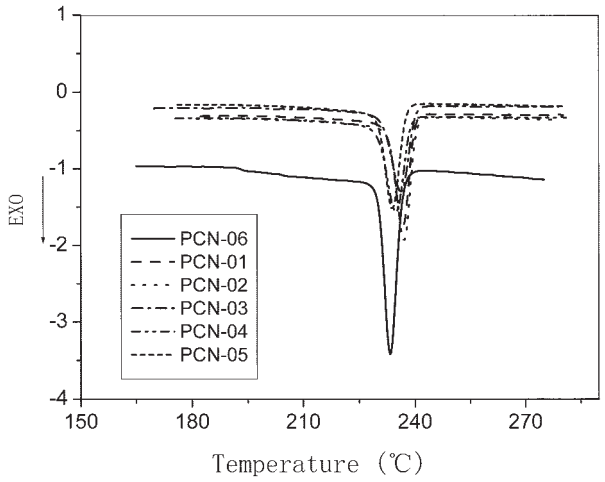

Figure 3 DSC cooling scans of samples.

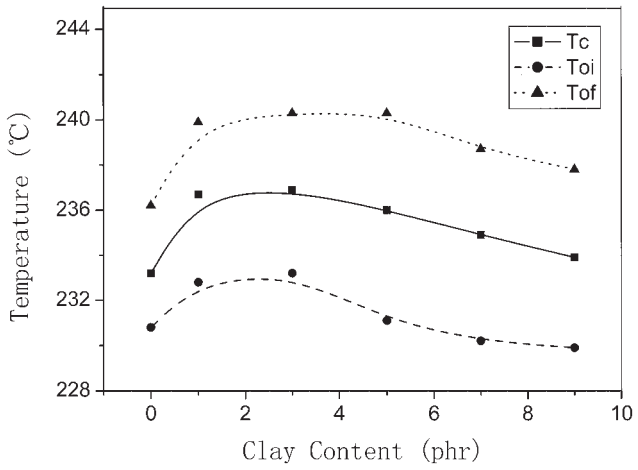

Figure 4 Relationship between crystallization temperatures and clay contents.

To obtain more information about the polymorphic behavior in PA 66/clay nanocomposites, nonisothermal crystallization experiments were conducted.

Relationship between the crystallization behaviors and the clay content

Figure 3 shows the influence of OMMT contents on the crystallization behaviors of PA 66. As seen from the figure, all samples have a single exothermic peak, but the shapes of those peaks and the crystallization temperatures are different. Data of crystallization thermodynamics parameters of PA 66 and its nanocomposites are shown in Table I. The results of Table I and Figure 3 indicate that the addition of OMMT in the matrix of PA 66 leads to increases of crystallization temperatures and FWHM of the exothermic peaks.

Figure 4 shows the relationship between crystallization temperatures and clay contents. As shown in Figure 4, the crystallization temperature is the highest when the clay content is 3 phr; the lowest temperature is that of pure PA 66, whereas that of PCN-05 is slightly higher than that of PA 66. Increases of crystallization temperatures illustrate that OMMTs act as nucleators of PA 66 and have heterogeneous nucleation effects on the matrix. Thus, the crystallization rate is clearly increased. Also, Figure 4 shows that the crystallization temperatures of nanocomposites decrease with the increase of the clay contents; that is because the large quantity of clay pellets cannot disperse uniformly within the matrix and thus finally agglomerate. These agglomerated clay pellets cannot act as a catalyst for nucleation.

The increases of FWHM of nanocomposites may be caused by two reasons:

1. The first possible reason is that the increase of the viscosity of the nanocomposites' system, which is caused by the large specific surface area and the strong interactivity between the modified silicate layers and the molecular chains of the matrix, results in the difficulty of movements of molecular chains, which leads to the decrease of crystal growth rate of PA 66. Because of the effect of heterogeneous nucleation, the crystal growth rate is the decisive step of the total crystallization rate. Thus, the decrease of crystal growth rate means the decrease of total crystallization rate. That is, crystallization needs more time and will experience a wider temperature range, which will lead to the

TABLE I
Crystallization Thermodynamics Parameters of PA 66 and Its Nanocomposites

Parameter	Sample					
	PCN-01	PCN-02	PCN-03	PCN-04	PCN-05	PCN-06
T_c, °C	236.7	236.9	236.0	234.9	233.9	233.2
T_{oi}, °C	232.8	233.2	231.1	230.2	229.9	230.8
T_{of}, °C	239.9	240.3	240.3	238.7	237.8	236.2
ΔT_c, °C	7.1	7.1	9.2	8.5	7.9	5.4
FWHM, °C	3.8	4.0	5.6	5.3	4.8	3.3
ΔH_m/J g^{-1}	−42.17	−46.62	−39.04	−43.19	−41.50	−56.79

TABLE II
MI of PA 66 and Its Nanocomposites

Parameter	Sample					
	PCN-01	PCN-02	PCN-03	PCN-04	PCN-05	PCN-06
MI, g/10 min	13.52	9.957	6.282	1.680	9.635×10^{-2}	11.38

increase of FWHM. Table II gives the melt indices (MI) of PA 66 and its nanocomposites. The results indicate that the viscosities of nanocomposites are increased with increasing clay contents, except for PCN-01.

2. The second possible reason is the inhomogeneity of the dispersions of silicate layers, which will result in the inhomogeneity of the crystal growth. As seen in Zhu et al.,[4] the TEM photograph of PCN-03 still shows signs of the original ordering of the silicate layers, although the thickness of most silicate layers is 10–50 nm. The molecular chains of PA 66 between the silicate layers and the chains in the region without silicate layers will have different crystal growth rates.

In fact, the special structure of silicate layers can also lead to the inhomogeneity of the crystal growth. For example, the chains on the face of silicate layers and the chains on the edges of silicate layers will have different crystal growth rates.

In conclusion, all those factors can result in the increase of FWHM of the exothermic peaks of PA 66 nanocomposites. However, the TEM photograph and the Molau experiments of our previous work[4] show that OMMTs in the PA 66 matrix have a reasonably satisfactory dispersion. Therefore, the viscosity factor constitutes the main influence on FWHM of the exothermic peaks of PA 66/clay nanocomposites.

Relationship between the half-crystallization time and the clay content

The point at which the exothermic peak of the crystallization DSC curve begins to deviate from the baseline is designated the initial point of time, t_0. Then, crystallinity X at time point t is obtained by the peak separation method, and a series of X–t curves are obtained (Fig. 5), as follows: at $X = 50\%$, draw a parallel line of t-axis and then draw droop lines of t-axis at the crossing points of X–t curves and the parallel line of t-axis. The crossing points of those droop lines and t-axis are half-crystallization times ($t_{1/2}$) of curves at different clay contents. Data are given in Table III. The results show that both $t_{1/2}$ and t_{max} (maximum crystallization time) are increased with increasing clay contents.

Plots of ln $t_{1/2}$ and ln t_{max} versus clay contents, respectively, are shown in Figure 6.

The results show that the relationships between ln $t_{1/2}$ and ln t_{max} versus clay contents are in both in good linear relation, indicating that $t_{1/2}$ and t_{max} are increased following an exponential relationship with the increasing clay content.

The two lines have similar slope coefficients and the intercepts are represented by the following equations:

$$\ln t_{1/2} = 0.024x - 0.3986 \quad (1)$$

$$\ln t_{max} = 0.029x - 0.4596 \quad (2)$$

where x is the clay content. Their transforms are expressed as

$$t_{1/2} = \exp(0.024x - 0.3986) \quad (3)$$

$$t_{max} = \exp(0.029x - 0.4596) \quad (4)$$

The relationship between $t_{1/2}$ and t_{max} can be obtained by the method in which eq. (3) is divided by eq. (4), as shown in the following equation:

$$t_{1/2}/t_{max} = 1.06 \exp(-0.005x) \quad (5)$$

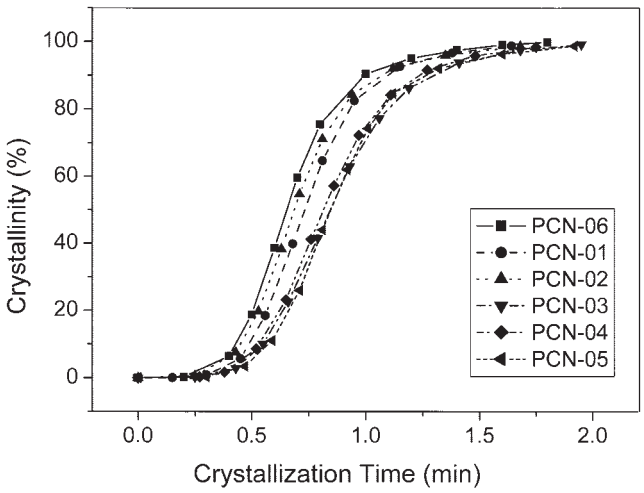

Figure 5 Development of crystallinity with time for nonisothermal crystallization of PA 66 and its nanocomposites.

TABLE III
Nonisothermal Crystallization Kinetic Parameters of PA 66/Clay Nanocomposites at Different Contents of Clay

Parameter	Sample					
	PCN-06	PCN-01	PCN-02	PCN-03	PCN-04	PCN-05
$t_{1/2}$, min	0.65	0.72	0.68	0.82	0.78	0.82
t_{max}, min	0.61	0.68	0.65	0.80	0.75	0.81
$D(k)$	3.8	4.2	4.5	5.7	5.4	5.2
lg Z_1	−4.01	−4.37	−4.14	−4.70	−4.78	−5.20
n_1	4.47	4.87	4.77	5.02	5.18	5.50
lg Z_2	−1.54	−2.17	−1.35	−1.94	−2.06	−1.34
n_2	1.89	2.37	1.64	2.05	2.18	1.54

Nonisothermal crystallization kinetic parameters

DSC is useful in the study of nonisothermal crystallization kinetics, although the processing methods are varied. Eopoxobckuü[22] proposed an approximate expression that is similar to the Avrami equation:

$$X = 1 - \exp[-Z(at)^n] \quad (6)$$

$$\lg Z = \lg Z_t - n \lg a \quad (7)$$

After logarithmic transformation, eq. (1) will change to the following format:

$$\lg[-\ln(1 - X)] = \lg Z + n \lg(at) \quad (8)$$

where X is the crystallinity at time t. By plotting the figure lg[−ln(1 − X)] versus lg(at), a line will be obtained. Its slope coefficient is the Avrami index n, and the intercept is the constant crystalline rate.

The Eopoxobckuű method is a quite reasonable way, so it is used in this article.

A plot of lg[−ln(1 − X)] versus lg(at) according to eq. (8), is shown in Figure 7.

As seen from Figure 7, lines are obtained at the initial crystallization periods of the PA 66 and its nanocomposites. However, there are turning points at their final crystallization periods and the final parts of crystallization periods also show linear relationships. The slope coefficients of the lines of the initial parts and the lines of the final parts differ. The fact that nonisothermal crystallization kinetic curves are fold lines indicates that there is secondary crystallization during the process of crystallization and that the mechanisms of core formation and growth of the crystal at different periods of the crystallization process are significantly different. The slope coefficients of the initial part and the final part are n_1 and n_2, whereas their intercepts are lg Z_1 and lg Z_2, respectively. Data of these variables are shown in Table III.

Within the framework of the Avrami system, the Avrami index n is the sum of space dimensions and time dimensions during the growth of crystal. As shown in Table III, n_1 shows a tend of increase as the increase of the clay contents, whereas lg Z_1 tends to decrease. The result indicates that the addition of clay influences the mechanism of core formation at the

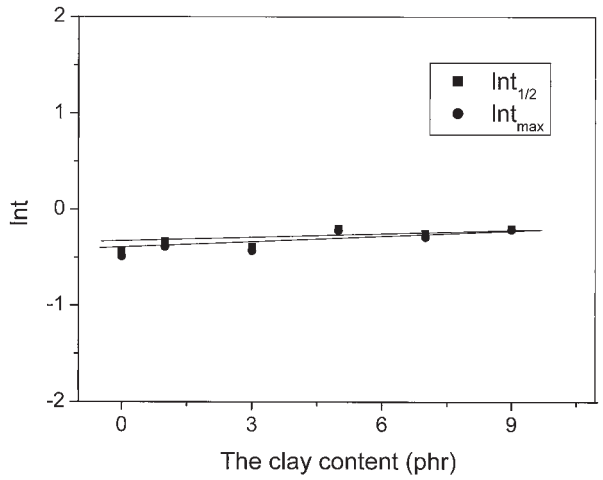

Figure 6 Plot of ln t versus the clay contents for nonisothermal crystallization of PA 66/clay nanocomposites.

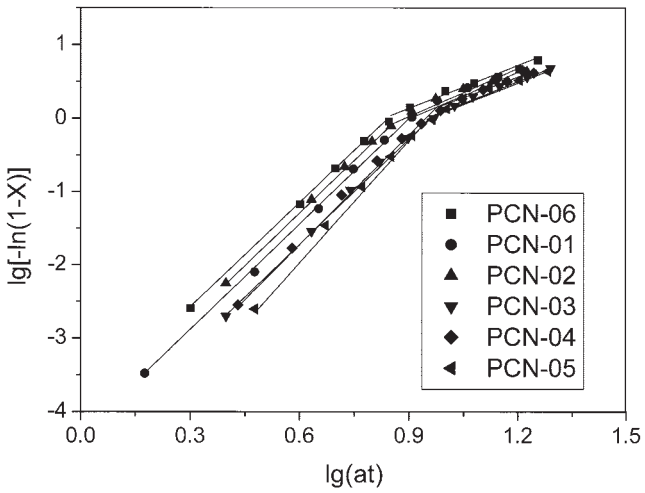

Figure 7 Plot of lg[−ln(1 − X)] versus lg(at) for crystallization of PA 66 and its nanocomposites.

initial part of crystallization. In the meanwhile, n_2 and lg Z_2 are not obviously influenced by the clay content. The average values of n_2 and lg Z_2 are 1.95 and -1.73, respectively. Such a result means that the modes of crystallization with different clay contents at the final part are driven to uniformity. Based on the relationships between the Avrami index and the different mechanisms of core formation and growth of crystallization,[23–27] it can be conjectured that the mechanism of crystallization at the initial part is heterogeneously fascicular three-dimensional growth ($n > 5$) or homogeneously spheric three-dimensional growth ($n = 4$), whereas at the final part it is two-dimensional ribbon growth ($n < 2$) or two-dimensional circular growth ($n = 2$), which is controlled by the diffusion process or one-dimensional striation growth ($n = 2$).

Morphology of PA 66 and its nanocomposites

Data of Avrami index n_1 in Table III show that n_1 values of PA 66/clay nanocomposites are higher than that of PA 66. The result indicates that the molecular chains of PA 66 intercalated into the interlayer spacings, effectively decreasing the potential barrier of the crystallization of PA 66. Moreover, the ratio between the length and the width of silicate layers of OMMT is very large, so the growth of crystal influenced by the structures of silicate layers changes in all directions during the crystallization.

The above-mentioned conjecture was confirmed by the PLM photographs. The pellets of PCN-06 and PCN-03 crystallized at 240°C, maintained for 10 min, and observed under a polarized-light microscope. As seen from Figures 8 and 9, the growth mode of crystal of PA 66 is primarily the spheric mode. The sizes of those crystals are large, although their distribution is not homogeneous. Even though the growth mode of PCN-03 crystals is still the spheric mode, the sizes of those crystals are small, and their distribution is uniform. The result indicates that the addition of layered silicate clay influences the mechanism of core formation and the mode of crystalline growth. The nanoscale particles exert a heterogeneous nucleation effect on the crystallization of the matrix, resulting in a decrease of the size of the spherocrystals.

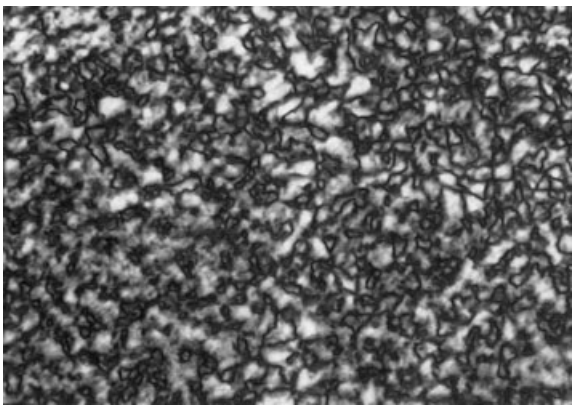

Figure 8 PLM photograph of nylon 66 sample.

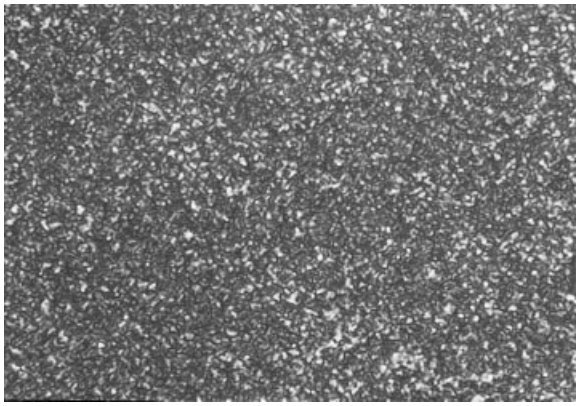

Figure 9 PLM photograph of PCN-03 sample.

CONCLUSIONS

1. The addition of OMMT can induce generation of the β-form crystal of PA 66 and substantially affect the arrangement of molecules in the α-form crystal. However, the addition of clay does not affect the crystallinities of PA 66 and its nanocomposites.
2. DSC results show that the addition of OMMT in the matrix of PA 66 leads to increases of crystallization temperatures and the full width at half maximum of the exothermic peaks. Moreover, the viscosity factor is the main influence on the FWHM of the exothermic peaks of PA 66/clay nanocomposites.

3 By adopting the Eopoxobckuű method, the nonisothermal crystallization kinetics of PA 66 and its nanocomposites were carefully studied, and it was found that the addition of layered silicate clay influences the mechanism of core formation and the mode of crystal growth. The nanoscale particles, which have the heterogeneous nucleation effect of the crystallization of the matrix, result in the decrease in size of the spherocrystal.

4. Photographs, obtained by polarized light microscopy, visually confirmed the above-mentioned results.

References

1. Ginzburg, V. V.; Singh, C.; Balazs, A. C. Macromolecules 2000, 33, 1089.

2. Vaia, R. A.; Price, G.; Ruth, P. N.; Nguyen, H. T. J Appl Clay Sci 1999, 15, 67.
3. Lincoln, D. M.; Vaia, R. A.; Wang, Z. G.; Hsiao, B. S. Polymer 2001, 42, 9975.
4. Zhu, C. S.; Kang, X.; He, S. Q.; Wang, L.; Liu, L. Chin J Polym Sci 2002, 20, 551.
5. Miyasaka, K.; Ishikawa, K. J Polym Sci A-2 1968, 6, 1317.
6. Miyasaka, K.; Ishikawa, K. J Polym Sci A-2 1972, 10, 1497.
7. Kyotani, M. J Macromol Sci Phys B 1975, 11, 509.
8. Murthy, N. S. Polym Commun 1991, 32, 301.
9. Murthy, N. S.; Curran, S. A.; Aharoni, S. M.; Minor, H. Macromolecules 1991, 24, 3215.
10. Brill, R. J. Prakt Chem 1942, 161, 49.
11. Starkweather, H. W., Jr. Macromolecules 1989, 22, 2000.
12. Hirschinger, J.; Miura, H.; Garder, K. H.; English, A. D. Macromolecules 1990, 23, 2153.
13. Androsch, R.; Stolp, M.; Radusch, H.-J. Acta Polym 1996, 47, 99.
14. Vasanthan, N.; Murthy, N. S.; Bray, R. G. Macromolecules 1998, 31, 8433.
15. Wu, T. M.; Wu, J. Y. J Macromol Sci Phys 2002, B41, 17.
16. Kohan, M. I. Nylon Plastics; Wiley New York, 1973.
17. Keller, A.; Maradudin, A. J Phys Chem Solids 1957, 2, 301.
18. Kamigaito, O. J Mater Res 1993, 8, 1174.
19. Kawasumi, M.; Kojima, Y.; Okada, A.; Kamigaito, O. U.S. Pat. 4,810,734 (1989).
20. Usuki, A.; Kojima, Y.; Kawasumi, M.; Okada, A.; Fukushima, Y.; Kurauchi, T.; Kamigaito, O. J Mater Res 1993, 8, 1179.
21. Usuki, A.; Kojima, Y.; Kawasumi, M.; Okada, A.; Kurauchi, T.; Kamigaito, O. Polym Prepr (Am Chem Soc Div Polym Chem) 1990, 31, 651.
22. Eopoxobckuű, B. A. Coeg Kpa Cool 1975, XVII, 35.
23. Avrami, M. J Chem Phys 1939, 7, 1103.
24. Hay, J. N.; Przekop, Z. J. J Polym Sci Polym Phys Ed 1979, 17, 951.
25. Morgan, L. B. J Appl Chem 1954, 4, 160.
26. Zhu, C. S., Pan, J. Y. Plast Proc Appl 1988, 4, 1.
27. Zhu, C. S., Pan, J. Y. Plast Proc Appl 1987, 4, 1.